Closed-Form 2D Angle Estimation With Rectangular Arrays Via DFT Beamspace ESPRIT[†]

Michael D. Zoltowski[†], *Martin Haardt*[‡], *and Cherian P. Mathews*[†]

[†] *School of Electrical Engineering*
Purdue University
West Lafayette, IN 47907-1285 USA

[‡] *Institute of Network Theory and Circuit Design*
Technical University of Munich
D-80290 Munich, Germany

ABSTRACT

UCA-ESPRIT is a recently developed closed form algorithm for use in conjunction with a uniform circular array (UCA) that provides automatically paired source azimuth and elevation angle estimates. *2D DFT Beamspace ESPRIT* is presented as an algorithm providing the same capabilities for a uniform rectangular array (URA). In the final stage of the algorithm, the real and imaginary parts of the *i-th* eigenvalue of a matrix yield the respective direction cosines of the *i-th* source relative to the two array axes. In addition to the reduction in computational complexity facilitated by operation in a reduced dimension beamspace, *2D DFT Beamspace ESPRIT* is efficiently formulated in terms of real-valued computation throughout. Simulation results are presented verifying the efficacy of the method.

1. INTRODUCTION

For 1D arrays, if the elements are uniformly-spaced, *Root-MUSIC* and *ESPRIT* avert a spectral search in determining the direction of arrival (DOA) of each incident signal. Instead, the DOA of each signal is determined from the roots of a polynomial. For either *Root-MUSIC* or *ESPRIT*[1], the roots of interest ideally lie on the unit circle and are related one-to-one with each source, assuming the interelement spacing to be less than or equal to a half-wavelength. For 2D (planar) arrays, the fact that the fundamental theorem of algebra does not hold in two dimensions typically precludes a rooting type of formulation. Even for the highly regular uniform rectangular array (URA), *2D MUSIC* requires a spectral search of a multimodal two-dimensional surface, while both *Multiple Invariance ESPRIT* [1] and Clark & Scharf's *2D IQML* [2] algorithm involve nonlinear optimization. Now, it should be pointed out that a URA lends itself to separable processing allowing one to decompose the 2D problem into two 1D problems. That is, one can estimate the DOA's with respect to one array axis via one set of calculations involving a *MUSIC* or *ESPRIT* based polynomial formulation, and do the same with respect to another array axis. Coupling information may be employed to subsequently pair the respective members of the two sets of 1D angle estimates.

In the Algebraically Coupled Matrix Pencil (*ACMP*) method of van der Veen *et al* eigenvector information is employed to pair the respective members of the two sets of 1D angle estimates. Yet, *ACMP* breaks down if two sources have the same arrival angle relative to either the x-axis or the y-axis, assuming the URA to lie in the x-y plane.

In contrast, for a uniform circular array (UCA) the recently developed *UCA-ESPRIT* [4] algorithm provides closed-form, automatically paired 2D angle estimates as long as the azimuth and elevation angle of each signal arrival is unique. In the final stage of *UCA-ESPRIT*, the *i-th* eigenvalue of a matrix is of the form $u_i + jv_i$, where u_i and v_i are the direction cosines of the *i-th* source relative to the x and y axes, respectively. These eigenvalues are unique for each source such that *UCA-ESPRIT* does not have the aforementioned problem *ACMP* has when two sources have the same u_i or the same v_i. We here develop a similar closed-form 2D angle estimation algorithm for a URA that provides automatic pairing in the same fashion. That is, in the final stage of new algorithm, referred to as *2D Unitary ESPRIT*, the real and imaginary parts of the *i-th* eigenvalue of a matrix are one-to-one related to u_i and v_i, respectively.

2. DFT BEAMSPACE ESPRIT FOR ULA

We begin the development by first developing a DFT beamspace version of *ESPRIT* for a uniform linear array (ULA) of N elements wherein each of the three primary steps of the algorithm are efficiently formulated in terms of real-valued computation: (1) the computation of the signal eigenvectors, (2) the solution to the system of equations derived from these signal eigenvectors, and (3) the computation of the eigenvalues of the solution to the system of equations formed in stage 2. Note that Xu *et. al.* [6] have also proposed a beamspace version of *ESPRIT* for a ULA. However, in their algorithm the three primary steps above involve complex-valued computation. The ability to formulate an *ESPRIT*-like algorithm for a ULA that only requires real-valued computations from start to finish, after the initial transformation from element space to beamspace, is critically important in developing a closed-form 2D angle estimation algorithm for a URA similar to *UCA-ESPRIT* for a UCA. Note, for the sake of notational simplicity, the following development employs all N DFT beams, so that the beamspace dimension is the same as that of element space. A reduced dimension beamspace version of the algorithm will be presented afterwards.

[†] This research was supported by NSF under grant no. MIP-9320890 and by AFOSR under contract no. F49620-92-J-0198.

[1] In *ESPRIT* the DOA's are extracted from eigenvalues which are roots of the characteristic polynomial of a matrix.

1058-6393/95 $4.00 © 1995 IEEE

Employing the center of the ULA as the phase reference, the array manifold is conjugate centro-symmetric [5]. For example, if the number of elements comprising the ULA, N, is odd, there is a sensor located at the array center and the array manifold is

$$\mathbf{a}_N(\mu) = \left[e^{-j(\frac{N-1}{2})\mu}, \ldots, e^{-j\mu}, 1, e^{j\mu} \ldots, e^{j(\frac{N-1}{2})\mu}\right]^T, \tag{1}$$

where $\mu = \frac{2\pi}{\lambda}du$ with λ equal to the wavelength, and d is equal to the interelement spacing. Applying the conjugate centro-symmetrized version of the $m-th$ row of the N pt. DFT matrix

$$\tilde{\mathbf{w}}_m^H = e^{j(\frac{N-1}{2})m\frac{2\pi}{N}}\left[1, e^{-jm\frac{2\pi}{N}}, e^{-j2m\frac{2\pi}{N}}, \ldots, e^{-j(N-1)m\frac{2\pi}{N}}\right]^T, \tag{2}$$

the $m-th$ component of the DFT beamspace manifold is

$$b_m(\mu) = \tilde{\mathbf{w}}_m^H \mathbf{a}_N(\mu) = \frac{\sin\left[\frac{N}{2}\left(\mu - m\frac{2\pi}{N}\right)\right]}{\sin\left[\frac{1}{2}\left(\mu - m\frac{2\pi}{N}\right)\right]}, \tag{3}$$

which is observed to be real-valued. Note that we can perform a front end FFT (effectively implementing the Vandermonde form of the rows of the DFT matrix) and achieve conjugate symmetrized beamforming a-posteriori through simple scaling of the DFT values [5]. The $N \times 1$ real-valued beamspace manifold is then

$$\mathbf{b}_N(\mu) = \tilde{\mathbf{W}}_N^H \mathbf{a}_N(\mu) = [b_0(\mu), b_1(\mu), \ldots, b_{N\text{-}1}(\mu)]^T, \tag{4}$$

where $\tilde{\mathbf{W}}_N^H$ denotes the conjugate centro-symmetrized N pt. DFT matrix whose rows are given by (2).

Comparing $b_{m+1}(\mu) = \frac{\sin\left[\frac{N}{2}\left(\mu-(m+1)\frac{2\pi}{N}\right)\right]}{\sin\left[\frac{1}{2}\left(\mu-(m+1)\frac{2\pi}{N}\right)\right]}$ with $b_m(\mu)$ in (3), the numerator of $b_{m+1}(\mu)$ is observed to be the negative of that of $b_m(\mu)$. Thus, two successive components of the beamspace manifold are related as

$$\sin\left[\frac{1}{2}\left(\mu - m\frac{2\pi}{N}\right)\right] b_m(\mu) + \sin\left[\frac{1}{2}\left(\mu - (m+1)\frac{2\pi}{N}\right)\right] b_{m+1}(\mu) = 0. \tag{5}$$

Trigonometric manipulations lead to

$$\tan\left(\frac{\mu}{2}\right)\left\{\cos\left(m\frac{\pi}{N}\right) b_m(\mu) + \cos\left((m+1)\frac{\pi}{N}\right) b_{m+1}(\mu)\right\} = \sin\left(m\frac{\pi}{N}\right) b_m(\mu) + \sin\left((m+1)\frac{\pi}{N}\right) b_{m+1}(\mu). \tag{6}$$

Compiling all $N-1$ equations in vector form yields

$$\tan\left(\frac{\mu}{2}\right)\boldsymbol{\Gamma}_1\mathbf{b}(\mu) = \boldsymbol{\Gamma}_2\mathbf{b}(\mu) \tag{7}$$

where

$$\boldsymbol{\Gamma}_1 = \begin{bmatrix} 1 & \cos\left(\frac{\pi}{N}\right) & 0 & \ldots & 0 & 0 \\ 0 & \cos\left(\frac{\pi}{N}\right) & \cos\left(\frac{2\pi}{N}\right) & \ldots & 0 & 0 \\ \vdots & \vdots & \vdots & \ddots & \vdots & \vdots \\ 0 & 0 & 0 & \ldots & \cos\left((\text{N-2})\frac{\pi}{N}\right) & \cos\left((\text{N-1})\frac{\pi}{N}\right) \end{bmatrix} \tag{8}$$

$$\boldsymbol{\Gamma}_2 = \begin{bmatrix} 0 & \sin\left(\frac{\pi}{N}\right) & 0 & \ldots & 0 & 0 \\ 0 & \sin\left(\frac{\pi}{N}\right) & \sin\left(\frac{2\pi}{N}\right) & \ldots & 0 & 0 \\ \vdots & \vdots & \vdots & \ddots & \vdots & \vdots \\ 0 & 0 & 0 & \ldots & \sin\left((\text{N-2})\frac{\pi}{N}\right) & \sin\left((\text{N-1})\frac{\pi}{N}\right) \end{bmatrix} \tag{9}$$

With d sources, the beamspace DOA matrix is $\mathbf{B} = [\mathbf{b}(\mu_1), \mathbf{b}(\mu_2), \ldots, \mathbf{b}(\mu_d)]$. The beamspace manifold relation in (7) translates into the beamspace DOA matrix relation

$$\boldsymbol{\Gamma}_1\mathbf{B}\boldsymbol{\Omega}_\mu = \boldsymbol{\Gamma}_2\mathbf{B}, \tag{10}$$

where

$$\boldsymbol{\Omega}_\mu = \text{diag}\left\{\tan\left(\frac{\mu_1}{2}\right), \ldots, \tan\left(\frac{\mu_d}{2}\right)\right\}. \tag{11}$$

Now, the appropriate signal eigenvectors for the algorithm presently under development may be computed as the "largest" left singular vectors of the real-valued matrix $[\mathcal{R}e\{\mathbf{Y}\}, \mathcal{I}m\{\mathbf{Y}\}]$, where $\mathbf{Y} = \tilde{\mathbf{W}}_N^H\mathbf{X}$. Asymptotically, the $N \times d$ matrix of signal eigenvectors, $\mathbf{E}_S$, satisfies $\mathbf{E}_S = \mathbf{BT}$, where $\mathbf{T}$ is an unknown $d \times d$ *real-valued* matrix. Substituting $\mathbf{B} = \mathbf{E}_S\mathbf{T}^{-1}$ into (10) yields the signal eigenvector relation

$$\boldsymbol{\Gamma}_1\mathbf{E}_S\boldsymbol{\Psi} = \boldsymbol{\Gamma}_2\mathbf{E}_S, \quad \text{where:} \quad \boldsymbol{\Psi} = \mathbf{T}^{-1}\boldsymbol{\Omega}_\mu\mathbf{T}. \tag{12}$$

Ultimately, the eigenvalues of the $d \times d$ solution $\boldsymbol{\Psi}$ to the $(N-1) \times d$ matrix equation above are $\tan(\mu_i/2)$ $i = 1, \ldots, d$.

This reveals a spatial frequency warping identical to the temporal frequency warping incurred in designing a digital filter from an analog filter via the bilinear transformation! Consider $d = \lambda/2$ so that $\mu = \frac{2\pi}{\lambda}du = \pi u$. In this case, there is a one-to-one mapping between $-1 < u_i < 1$, corresponding to the range of possible values for a direction cosine, and $-\infty < \omega_i < \infty$.

A summary of *DFT Beamspace ESPRIT* is as follows. First, compute an N pt. DFT of each snapshot vector thereby forming $\mathbf{Y} = \tilde{\mathbf{W}}_N^H\mathbf{X}$. Second, compute $\mathbf{E}_s$ via the d "largest" left singular vectors of the real-valued matrix $[\mathcal{R}e\{\mathbf{Y}\}, \mathcal{I}m\{\mathbf{Y}\}]$. Third, compute $\boldsymbol{\Psi}$ (via LS or TLS) as the solution to the $(N-1) \times d$ matrix equation $(\boldsymbol{\Gamma}_1\mathbf{E}_S)\boldsymbol{\Psi} = (\boldsymbol{\Gamma}_2\mathbf{E}_S)$. Fourth, compute ω_i, $i = 1, \ldots, d$, as the eigenvalues of the $d \times d$ real-valued matrix $\boldsymbol{\Psi}$. Finally, the spatial frequency estimates are $\mu_i = 2\tan^{-1}(\omega_i)$ $i = 1, \ldots, d$.

Reduced computational complexity is realized in scenarios where one works with DFT beams that encompass some angular sector of interest. In this case, one only employs a subset of the rows of $\tilde{\mathbf{W}}_N^H$, the number of which depends on the width of that sector and may be substantially less than N, to transform from element space to beamspace. Employing the appropriate subblocks of $\boldsymbol{\Gamma}_1$ and $\boldsymbol{\Gamma}_2$ as selection matrices, the algorithm is the same as that summarized previously except for the reduced dimensionality. For example, if one employed the *m-th*, *(m+1)-th*, and *(m+2)-th* rows of $\tilde{\mathbf{W}}_N^H$ to form three beams to estimate the angles of two closely-spaced signal arrivals, as in the low-angle radar tracking scheme described by Zoltowski and Lee [8], for example, the appropriate 2×3 selection matrices are

$$\boldsymbol{\Gamma}_1 = \begin{bmatrix} \cos\left(m\frac{\pi}{N}\right) & \cos\left((m+1)\frac{\pi}{N}\right) & 0 \\ 0 & \cos\left((m+1)\frac{\pi}{N}\right) & \cos\left((m+2)\frac{\pi}{N}\right) \end{bmatrix}$$

$$\mathbf{\Gamma}_2 = \begin{bmatrix} \sin\left(m\frac{\pi}{N}\right) & \sin\left((m+1)\frac{\pi}{N}\right) & 0 \\ 0 & \sin\left((m+1)\frac{\pi}{N}\right) & \sin\left((m+2)\frac{\pi}{N}\right) \end{bmatrix}.$$

In this case, one would compute the $d = 2$ "largest" eigenvectors of a 3×3 real-valued matrix, solve a 2×2 real-valued system of equations, and compute the 2 eigenvalues of the resulting 2×2 matrix solution.

3. 2D DFT BEAMSPACE ESPRIT FOR URA

We now extend 1D DFT Beamspace ESPRIT for a uniform rectangular array (URA) of $N \times M$ elements lying in the x-y plane and equi-spaced by d in either the x or y directions. In addition to $\mu = \frac{2\pi}{\lambda}du$, where u is the direction cosine variable relative to the x-axis, we define the spatial frequency variable $\nu = \frac{2\pi}{\lambda}dv$, where v is the direction cosine variable relative to the y-axis.

In this development, in addition to representing the array manifold as an $NM \times 1$ vector, denoted $\mathbf{a}(\mu,\nu)$, it will be convenient to represent it as an $N \times M$ matrix, denoted $\mathcal{A}(\mu,\nu)$, as well. The two forms are related through the operators $vec(\cdot)$ and $mat(\cdot)$ as $\mathbf{a}(\mu,\nu) = vec(\mathcal{A}(\mu,\nu))$ and $\mathcal{A}(\mu,\nu) = mat(\mathbf{a}(\mu,\nu))$. The operator $vec(\cdot)$ maps an $N \times M$ matrix to an $NM \times 1$ vector by stacking the columns of the matrix. The operator $mat(\cdot)$ performs the inverse mapping, mapping an $NM\times1$ vector into an $N\times M$ matrix such that that $mat(vec(\mathbf{X})) = \mathbf{X}$. An important property of the vec operator that will prove useful throughout the development is

$$vec(\mathbf{ABC}) = (\mathbf{C}^T \otimes \mathbf{A})\ vec(\mathbf{B}), \tag{13}$$

where $\otimes$ denotes the Kronecker matrix product. In matrix form, the array manifold may be expressed as

$$\mathcal{A}(\mu,\nu) = \mathbf{a}_N(\mu)\mathbf{a}_M^T(\nu), \tag{14}$$

where $\mathbf{a}_M(\nu)$ is defined by (1) with N replaced by M and μ replaced by ν.

The matrix form of the beamspace manifold, denoted $\mathcal{B}(\mu,\nu)$, is related to the matrix form of the array manifold via a 2D DFT as $\mathcal{B}(\mu,\nu) = \tilde{\mathbf{W}}_N^H\mathcal{A}(\mu,\nu)\tilde{\mathbf{W}}_M^*$, where $\tilde{\mathbf{W}}_N^H$ denotes the conjugate centro-symmetrized N pt. DFT matrix whose rows are given by (2) and $\tilde{\mathbf{W}}_M^H$ is defined similarly with N replaced by M. Substituting the form of $\mathcal{A}(\mu,\nu)$ in (31) into $\mathcal{B}(\mu,\nu) = \tilde{\mathbf{W}}_N^H\mathcal{A}(\mu,\nu)\tilde{\mathbf{W}}_M$ yields

$$\mathcal{B}(\mu,\nu) = \mathbf{b}_N(\mu)\mathbf{b}_M^T(\nu), \tag{15}$$

where $\mathbf{b}_N(\mu)$ is defined in (4) and $\mathbf{b}_M(\nu)$ is defined similarly with N replaced by M and μ replaced by ν. Given that $\mathbf{b}_N(\mu)$ satisfies the invariance relationship in (7), it follows that $\mathcal{B}(\mu,\nu)$ satisfies

$$\tan\left(\frac{\mu}{2}\right)\ \mathbf{\Gamma}_1 B(\mu,\nu) = \mathbf{\Gamma}_2 B(\mu,\nu). \tag{16}$$

where $\mathbf{\Gamma}_1$ and $\mathbf{\Gamma}_2$ are defined in (8) and (9). Using the property of the vec operator in (13), we find that the $NM\times 1$ beamspace manifold in vector form, denoted $\mathbf{b}(\mu,\nu) = vec(\mathcal{B}(\mu,\nu))$, satisfies

$$\tan\left(\frac{\mu}{2}\right)\ \mathbf{\Gamma}_{\mu1}\mathbf{b}(\mu,\nu) = \mathbf{\Gamma}_{\mu2}\mathbf{b}(\mu,\nu), \tag{17}$$

where $\mathbf{\Gamma}_{\mu1}$ and $\mathbf{\Gamma}_{\mu2}$ are the $(N-1)M \times NM$ matrices:

$$\mathbf{\Gamma}_{\mu1} = \mathbf{I}_M \otimes \mathbf{\Gamma}_1 \quad \text{and} \quad \mathbf{\Gamma}_{\mu2} = \mathbf{I}_M \otimes \mathbf{\Gamma}_2. \tag{18}$$

(17) represents $(N-1)M$ equations obtained by comparing each pair of adjacent beams having the same ν pointing angle coordinate.

Similarly, the 1D beamspace manifold $\mathbf{b}_M(\nu)$ satisfies $\tan(\nu/2)\ \mathbf{\Gamma}_3\mathbf{b}_M(\nu) = \mathbf{\Gamma}_4\mathbf{b}_M(\nu)$, where $\mathbf{\Gamma}_3$ and $\mathbf{\Gamma}_4$ are defined similar to (8) and (9) with N replaced by M such that they are $(M-1)\times M$. It follows that

$$\tan\left(\frac{\nu}{2}\right)\ B(\mu,\nu)\mathbf{\Gamma}_3^T = B(\mu,\nu)\mathbf{\Gamma}_4^T. \tag{19}$$

Again, using the vec operator, we find that $\mathbf{b}(\mu,\nu)$ satisfies

$$\tan\left(\frac{\nu}{2}\right)\ \mathbf{\Gamma}_{\nu1}\mathbf{b}(\mu,\nu) = \mathbf{\Gamma}_{\nu2}\mathbf{b}(\mu,\nu), \tag{20}$$

where $\mathbf{\Gamma}_{\nu1}$ and $\mathbf{\Gamma}_{\nu2}$ are the $N(M-1)\times NM$ matrices:

$$\mathbf{\Gamma}_{\nu1} = \mathbf{\Gamma}_3 \otimes \mathbf{I}_N \quad \text{and} \quad \mathbf{\Gamma}_{\nu2} = \mathbf{\Gamma}_4 \otimes \mathbf{I}_N. \tag{21}$$

(20) represents $N(M-1)$ equations obtained by comparing each pair of adjacent beams having the same μ pointing angle coordinate.

Consider the $NM\times d$ real-valued beamspace DOA matrix $\mathbf{B} = [\mathbf{b}(\mu_1,\nu_1),...,\mathbf{b}(\mu_d,\nu_d)]$. (17) dictates that $\mathbf{B}$ satisfies

$$\mathbf{\Gamma}_{\mu1}\mathbf{B}\mathbf{\Omega}_\mu = \mathbf{\Gamma}_{\mu2}\mathbf{B} \tag{22}$$

where $\mathbf{\Omega}_\mu$ is defined in (11). In turn, (20) dictates that $\mathbf{B}$ satisfies

$$\mathbf{\Gamma}_{\nu1}\mathbf{B}\mathbf{\Omega}_\nu = \mathbf{\Gamma}_{\nu2}\mathbf{B} \tag{23}$$

where

$$\mathbf{\Omega}_\nu = \operatorname{diag}\left\{\tan\left(\frac{\nu_1}{2}\right),...,\tan\left(\frac{\nu_d}{2}\right)\right\}. \tag{24}$$

Now, viewing the array output at a given snapshot as an $N\times M$ matrix, we compute a 2D DFT, apply the vec operator, and place the resulting $NM\times1$ vector as a column of an $NM\times N_s$ data matrix $\mathbf{Y}$. Recall that $\mathbf{X}$ denotes the $NM\times N_s$ data matrix prior to the 2D DFT. Using the vec operator, the relationship between $\mathbf{Y}$ and $\mathbf{X}$ may be expressed as $\mathbf{Y} = (\tilde{\mathbf{W}}_M^H \otimes \tilde{\mathbf{W}}_N^H)\mathbf{X}$. The appropriate $NM\times d$ matrix of signal eigenvectors, $\mathbf{E}_S$, for the algorithm presently under development may be computed as the d "largest" left singular vectors of the real-valued matrix $[\mathcal{R}e\{\mathbf{Y}\},\mathcal{I}m\{\mathbf{Y}\}]$. Asymptotically, $\mathbf{E}_S = \mathbf{BT}$, where $\mathbf{T}$ is an unknown $d\times d$ *real-valued* matrix. Substituting $\mathbf{B} = \mathbf{E}_S\mathbf{T}^{-1}$ into (22) and (23) yields the signal eigenvector relations

$$\mathbf{\Gamma}_{\mu1}\mathbf{E}_S\mathbf{\Psi}_\mu = \mathbf{\Gamma}_{\mu2}\mathbf{E}_S \quad \text{where:} \quad \mathbf{\Psi}_\mu = \mathbf{T}^{-1}\mathbf{\Omega}_\mu\mathbf{T} \tag{25}$$

$$\mathbf{\Gamma}_{\nu1}\mathbf{E}_S\mathbf{\Psi}_\nu = \mathbf{\Gamma}_{\nu2}\mathbf{E}_S \quad \text{where:} \quad \mathbf{\Psi}_\nu = \mathbf{T}^{-1}\mathbf{\Omega}_\nu\mathbf{T}. \tag{26}$$

Automatic pairing of μ and ν spatial frequency estimates is facilitated by the fact that all of the quantities in (25) and (25) are real-valued. Thus, $\mathbf{\Psi}_\mu + j\mathbf{\Psi}_\nu$ may be spectrally decomposed as

$$\mathbf{\Psi}_\mu + j\mathbf{\Psi}_\nu = \mathbf{T}^{-1}\left\{\mathbf{\Omega}_\mu + j\mathbf{\Omega}_\nu\right\}\mathbf{T} \tag{27}$$

A summary of *2D DFT Beamspace ESPRIT* is as follows. First, compute a 2D DFT of the $N \times M$ matrix of array outputs at each snapshot, apply the *vec* operator, and place the result as a column of $\mathbf{Y}$. Second, compute $\mathbf{E}_s$ via the d "largest" left singular vectors of the real-valued matrix $[\mathcal{R}e\{\mathbf{Y}\}, \mathcal{I}m\{\mathbf{Y}\}]$. Third, compute (via LS or TLS) $\mathbf{\Psi}_\mu$ as the solution to the $(N-1)M \times d$ matrix equation $\mathbf{\Gamma}_{\mu 1}\mathbf{E}_S\mathbf{\Psi}_\mu = \mathbf{\Gamma}_{\mu 2}\mathbf{E}_S$ and $\mathbf{\Psi}_\nu$ as the solution to the $N(M-1) \times d$ matrix equation $\mathbf{\Gamma}_{\nu 1}\mathbf{E}_S\mathbf{\Psi}_\nu = \mathbf{\Gamma}_{\nu 2}\mathbf{E}_S$. Fourth, compute λ_i, $i = 1, ..., d$, as the eigenvalues of the $d \times d$ complex-valued matrix $\mathbf{\Psi}_\mu + j\mathbf{\Psi}_\nu$. Finally, the spatial frequency estimates are $\mu_i = 2\tan^{-1}(\mathcal{R}e\{\lambda_i\})$ and $\nu_i = 2\tan^{-1}(\mathcal{I}m\{\lambda_i\})$, $i = 1, ..., d$.

3.1. Reduced Dimension Example

As in the 1D case, the utility of *2D DFT Beamspace ESPRIT* over *2D Unitary ESPRIT* is in scenarios where one works with 2D DFT beams that encompass some volume of space of interest. In fact, the ability to work in a reduced dimension beamspace is even of more value in the case of a URA since the total number of elements may be quite high. As an example, consider a scenario, similar to the low-angle radar tracking problem, in which we desire to estimate the respective azimuth and elevation angles of each of two closely-spaced sources. Suppose that we form four 2D DFT beams steered to the spatial frequency coordinate pairs $(m\frac{2\pi}{N}, n\frac{2\pi}{M})$, $((m+1)\frac{2\pi}{N}, n\frac{2\pi}{M})$, $(m\frac{2\pi}{N}, (n+1)\frac{2\pi}{M})$, and $((m+1)\frac{2\pi}{N}, (n+1)\frac{2\pi}{M})$; the 4×1 beamspace manifold is

$$\mathbf{b}(\mu,\nu) = \tag{28}$$

$$\left[b_{m,n}(\mu,\nu)\,, b_{m+1,n}(\mu,\nu)\,, b_{m,n+1}(\mu,\nu)\,, b_{m+1,n+1}(\mu,\nu)\right]^T.$$

In this case, $\mathbf{E}_S$ is 4×2 and may be constructed from the two "largest" eigenvectors of the real part of the 4×4 matrix formed from the inter-beam correlations. The 2×2 matrices $\mathbf{\Psi}_\mu$ and $\mathbf{\Psi}_\nu$ would be computed as the corresponding solutions to the 2×2 respective matrix equations $\mathbf{\Gamma}_{\mu 1}\mathbf{E}_S\mathbf{\Psi}_\mu = \mathbf{\Gamma}_{\mu 2}\mathbf{E}_S$ and $\mathbf{\Gamma}_{\nu 1}\mathbf{E}_S\mathbf{\Psi}_\nu = \mathbf{\Gamma}_{\nu 2}\mathbf{E}_S$, where

$$\mathbf{\Gamma}_{\mu 1} =$$

$$\begin{bmatrix} \cos\left(m\frac{\pi}{N}\right) & \cos\left((m+1)\frac{\pi}{N}\right) & 0 & 0 \\ 0 & 0 & \cos\left(m\frac{\pi}{N}\right) & \cos\left((m+1)\frac{\pi}{N}\right) \end{bmatrix}$$

$$\mathbf{\Gamma}_{\mu 2} =$$

$$\begin{bmatrix} \sin\left(m\frac{\pi}{N}\right) & \sin\left((m+1)\frac{\pi}{N}\right) & 0 & 0 \\ 0 & 0 & \sin\left(m\frac{\pi}{N}\right) & \sin\left((m+1)\frac{\pi}{N}\right) \end{bmatrix}$$

$$\mathbf{\Gamma}_{\nu 1} =$$

$$\begin{bmatrix} \cos\left(n\frac{\pi}{N}\right) & 0 & \cos\left((n+1)\frac{\pi}{N}\right) & 0 \\ 0 & \cos\left(n\frac{\pi}{N}\right) & 0 & \cos\left((n+1)\frac{\pi}{N}\right) \end{bmatrix}$$

$$\mathbf{\Gamma}_{\nu 2} =$$

$$\begin{bmatrix} \sin\left(n\frac{\pi}{N}\right) & 0 & \sin\left((n+1)\frac{\pi}{N}\right) & 0 \\ 0 & \sin\left(n\frac{\pi}{N}\right) & 0 & \sin\left((n+1)\frac{\pi}{N}\right) \end{bmatrix}.$$

In the final stage, $\tan(\mu_i/2) + j\tan(\nu_i/2)$, $i = 1, 2$, would be computed as the the eigenvalues of a 2×2 matrix.

As discussed previously, *UCA-ESPRIT* [4] is a recently developed closed-form 2D angle estimation scheme for a uniform circular array (UCA). In the final stage of *UCA-ESPRIT*, the *i-th* eigenvalue of a matrix has the form $u_i + jv_i$, where u_i and v_i are the direction cosines of the *i-th* source relative to the x and y axes, respectively, assuming the UCA to lie in the x-y plane. This is in contrast to *2D DFT Beamspace ESPRIT* where there is spatial frequency warping such that the final eigenvalues are of the form $\tan(\mu_i/2) + j\tan(\nu_i/2)$, $i = 1, ..., d$. A notable difference between the development of *UCA-ESPRIT* and that of *2D DFT Beamspace ESPRIT* is that in the former the sampled aperture pattern was assumed to be approximately equal to the continuous aperture pattern [4], while no such approximation was made in the latter case. It has been shown in [9] that if a similar approximation is made in the development of *2D DFT Beamspace ESPRIT*, the final eigenvalues yielded by the resulting approximate *2D DFT Beamspace ESPRIT* algorithm are identical in form to those yielded by *UCA-ESPRIT*. Aside from averting spatial frequency warping, this form of the eigenvalue has a nice geometrical interpretation in that it may be expressed as $u_i + jv_i = \sin\theta_i\, e^{j\phi_i}$, where ϕ_i and θ_i are the azimuth and elevation angles of the *i-th* source. θ_i varies between 0° and 90° so that $\sin\theta_i$ varies between 0 and 1, while ϕ_i varies between 0° and 360°. Thus, one can immediately glean the azimuth angle of the *i-th* source from the polar angle of the *i-th* eigenvalue, and the corresponding elevation angle from the arcsine of the magnitude of the *i-th* eigenvalue. If the eigenvalue is at the origin, the source is at boresite. If the eigenvalue is on the unit circle, the source is in the same plane as the array. Also, we may use the fact that an eigenvalue should be located on or within the unit circle to screen out false alarms.

4. SIMULATIONS

Simulations were conducted employing an 8×8 URA (*i.e.* , $N = M = 8$) with $\Delta_x = \Delta_y = \lambda/2$. The source scenario consisted of $d = 3$ equi-powered, uncorrelated sources located at $(u_1, v_1) = (0, 0)$, $(u_2, v_2) = (1/8, 0)$, and $(u_3, v_3) = (0, 1/8)$, where u_i and v_i are the direction cosines of the *i-th* source relative to the x and y axes, respectively. Sources 1 and 2 were separated by a half-beamwidth, *i. e.*, half the Rayleigh resolution limit, as were sources 2 and 3. Sources 1 and 2 have the same v coordinate, while sources 2 and 3 have the same u coordinate. If the *ACMP* algorithm of van der Veen *et al* [3] was applied in this scenario, it would provide a faulty estimate of the number of sources as well as faulty source direction estimates.

A given trial run at a given SNR level (per source per element) involved $N_s = 64$ snapshots. The noise was *i.i.d.* from element to element and from snapshot to snapshot. The RMS error was employed as the performance metric. Let $(\hat{u}_{i_k}, \hat{v}_{i_k})$ denote the coordinate estimates of the *i-th* source obtained from a particular algorithm at the *k-th* run. Sample performance statistics were computed from $K = 500$ independent trials as

$$\widehat{RMSE}_i = \sqrt{\frac{1}{K}\sum_{k=1}^{K}\left\{(\hat{u}_{i_k} - u_i)^2 + (\hat{v}_{i_k} - v_i)^2\right\}}\,,\ i = 1, 2, 3. \tag{29}$$

The bias of *2D DFT Beamspace ESPRIT* for $N_s = 64$ snapshots over the range of SNR's simulated was found to be negligible. This facilitated comparison with the Cramer Rao Lower Bound (CRLB). The performance of *2D DFT Beamspace ESPRIT* relative to *2D MUSIC* was also compared. The CRLB and the theoretically predicted performance of *2D MUSIC* were computed according to formulas provided in [4] and are plotted in Figures 1(a), 1(b), and 1(c) for sources 1, 2, and 3, respectively. Finally, for purposes of comparison, the relative performance of *2D Unitary ESPRIT* [9] is included in the plots. *2D Unitary ESPRIT* is a closed-form 2D angle estimation technique similar to *2D DFT Beamspace ESPRIT* but based in element space and thereby not lending itself to reduced dimension beamspace processing.

Note that *2D MUSIC* essentially achieved the CRLB over the range of SNR's simulated so that its theoretically predicted RMSE curve is coincident with the CRLB curve. Of course, *2D MUSIC* requires the localization of 3 peaks of a 2D spectrum. In element space, determining the value of the *2D MUSIC* spectrum at a given point involves the calculation of an inner product of the form $\mathbf{a}^H(\mu,\nu)\mathbf{P}^{\perp}\mathbf{a}(\mu,\nu)$, where $\mathbf{P}^{\perp}$ is 64×64. This kind of calculation has to be done repeatedly in performing a localized Newton-Raphson search around each spectral peak.

The respective RMSE's of *2D Unitary ESPRIT* and *2D DFT Beamspace ESPRIT* for sources 1, 2, and 3 are plotted in Figures 1(a), 1(b), and 1(c), respectively. For the *2D Unitary ESPRIT* algorithm developed in [9], the computations required for a single run were: (i) 64 additions per each of 64 snapshots to transform from complex-valued space to real-valued space, (ii) calculation of the 3 "largest" left singular vectors of a 64×128 real-valued matrix, (iii) calculation of the solution to two systems of equations of the form $\mathbf{AX} = \mathbf{B}$ where $\mathbf{A}$ and $\mathbf{B}$ are both 64×3 and real-valued, and (iv) calculation of the eigenvalues of a 3×3 complex-valued matrix. The performance of *2D Unitary ESPRIT* is observed to be very close to the CRLB for SNR's greater than or equal to -6 dB, although it does not achieve the CRLB even at the rather high SNR level of 12 dB. (Keep in mind that there are 64 elements and that the SNR is that per element.) Observe that on a logarithmic scale, the small gap between the performance of *2D Unitary ESPRIT* and the CRLB is fairly constant as a function of SNR for SNR's above -6 dB.

To demonstrate the efficacy of working in a reduced dimension beamspace, *2D DFT Beamspace ESPRIT* employed a 3×3 set of 9 beams with mainlobes rectangularly spaced in the u-v plane and centered at $(u, v) = (0, 0)$. In accordance with the summary of *2D DFT Beamspace ESPRIT* at the end of Section 4.0, the computations required for a single run were: (i) 9 sets of 64 multiplications and 63 additions for each of 64 snapshots to transform from element space to beamspace, (ii) calculation of the 3 "largest" left singular vectors of a 9×128 real-valued matrix, (iii) calculation of the solution to two systems of equations of the form $\mathbf{AX} = \mathbf{B}$ where $\mathbf{A}$ and $\mathbf{B}$ are both 6×3 and real-valued, and (iv) calculation of the eigenvalues of a 3×3 complex-valued matrix. A scatter plot of the 3 eigenvalues obtained from *2D DFT Beamspace ESPRIT* for each of 200 independent runs at an SNR of 3 dB is displayed in Figure 4(d). For SNR's greater than or equal to -6 dB, the performance of *2D DFT Beamspace ESPRIT* is observed to be only slightly worse than that of *2D Unitary ESPRIT* despite the dramatic reduction in computational complexity.

The difference in performance between *2D Unitary ESPRIT* or *2D DFT Beamspace ESPRIT* and the CRLB, and the fact that *2D MUSIC* achieves the CRLB for the range of SNR's simulated, suggests a strategy wherein the 2D angle estimates provided by either algorithm are used as starting points for localized Newton searches of the *2D MUSIC* spectrum to achieve uniformly minimum variance unbiased estimates (UMVUE's). Note that the computational burden of performing these localized searches of the *2D MUSIC* spectrum may be reduced substantially by operating in a reduced dimension, real-valued beamspace.

REFERENCES

[1] A. L. Swindlehurst, B. Ottersten, G. Xu, R. H. Roy, and T. Kailath, "Multiple Invariance ESPRIT", *IEEE Trans. Signal Processing*, pp. 867-881, Apr. 1992.

[2] M. P. Clark and L. L. Scharf, "Two-Dimensional Modal Analysis Based on Maximum Likelihood", *IEEE Trans. Signal Process.*, pp. 1443-1452, Jun. 1994.

[3] A.J. van der Veen, P.B. Ober, E.D. Deprettere, "Azimuth and Elevation Computation in High Resolution DOA Estimation", *IEEE Trans. Signal Processing*, vol. 40, pp. 1828-1832, July 1992.

[4] C.P. Mathews and M.D. Zoltowski, "Eigenstructure Techniques for 2-D Angle Estimation with Uniform Circular Arrays," *IEEE Trans. on Signal Processing*, vol. 42, pp. 2395-2407. Sept. 1994.

[5] M.D. Zoltowski, G.M. Kautz, and S.D. Silverstein, "Beamspace Root-MUSIC", *IEEE Trans. Signal Processing*, vol. 41, pp. 344-364, Jan. 1993.

[6] G. Xu, S.D. Silverstein, R. H. Roy, and T. Kailath, "Beamspace ESPRIT," *IEEE Trans. Signal Processing*, vol. 42, pp. 349-356, Feb. 1994.

[7] G. Xu, R.H. Roy, and T. Kailath, "Detection of Number of Sources via Exploitation of Centro-symmetry Property", *IEEE Trans. Signal Processing*, vol. 42, pp. 102-112, Jan. 1994.

[8] M. D. Zoltowski and T. Lee, "Maximum Likelihood Based Sensor Array Signal Processing in the Beamspace Domain for Low-Angle Radar Tracking," *IEEE Trans. on Signal Processing*, vol. 39, pp. 656-671, Mar. 1991.

[9] M. D. Zoltowski, M. Haardt, and C. P. Mathews, "Closed-Form 2D Angle Estimation with Rectangular Arrays in Element Space or Beamspace Via Unitary ESPRIT," submitted to *IEEE Trans. on Signal Processing*.

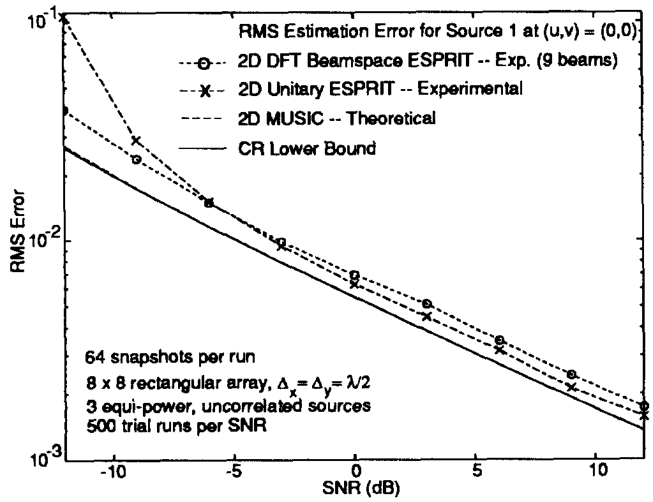

Figure 1: (a) RMSE for source 1 in simulation example.

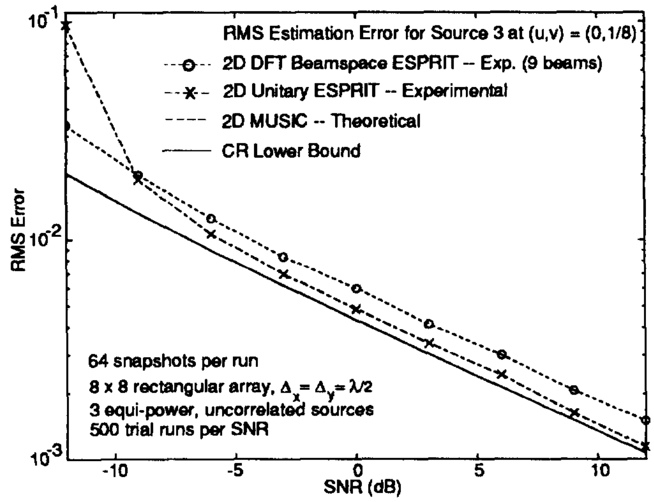

Figure 1: (c) RMSE for source 3 in simulation example.

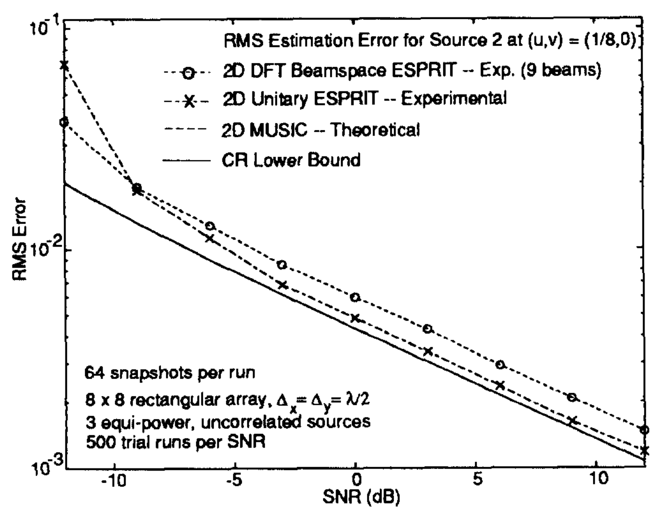

Figure 1: (b) RMSE for source 2 in simulation example.

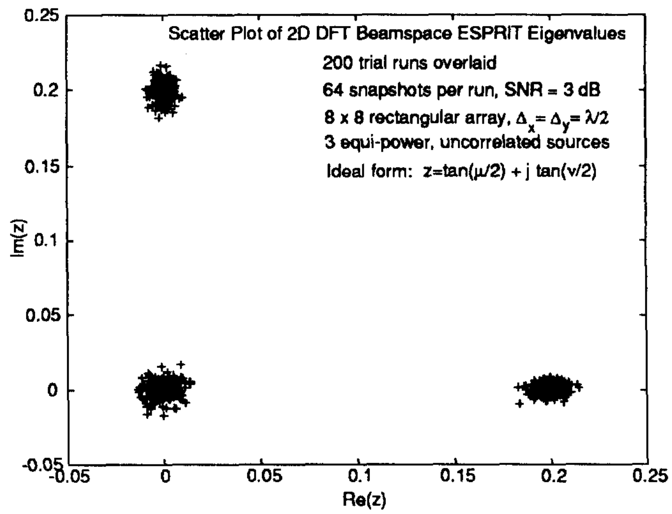

Figure 1: (d) Scatter plot of 2D DFT Beamspace ESPRIT eigenvalues.